ISA Journal of Engineering and Technology (ISAJET)

Homepage: https://isapublisher.com/isajet/

Volume 3, Issue 3, May-Jun, 2026 ISSN: 3049-1843

Research on Key Technologies for Reinforcement of Soft Foundation in Loess Tunnels

MD Wahiduzzaman

Southwest Jiaotong University

Received: *11.04.2026* **|** ***Accepted:*** *15.05.2026* **|** ***Published:*** *16.05.2026*

***Corresponding Author:** MD Wahiduzzaman

DOI: *10.5281/zenodo.20225914*

Abstract **Conference**

Loess tunnels in China's Loess Plateau face significant stability challenges due to the collapsible nature and moisture sensitivity of loess. This study investigates foundation behavior and reinforcement design for plain concrete pile composite foundations through integrated laboratory testing and three-dimensional numerical simulation. Laboratory tests quantified moisture-dependent mechanical properties: cohesion decreases from 43.33 kPa (w=14%) to 36.26 kPa (w=20%), following $c = 59.5 - 1.17w$ (R^2=0.99), while friction angle decreases from 33.7° to 29.4° following $\varphi = 43.7 - 0.72w$ (R^2=0.996). Interface shear tests revealed loess-concrete adhesion ratios (ca/c) of 0.25–0.30 at natural moisture, critical for pile shaft capacity calculations. Three-dimensional finite element models simulated excavation-support processes across burial depths of 5–46 m. Contact pressure exhibits non-uniform distribution with peak values of 1.32–1.42×γH at arch feet. The empirical relationship $\sigma\_base,peak = \eta \times \gamma H$, where $\eta = 1.12 + 0.0077H$ (R^2=0.89), provides a practical tool for foundation pressure prediction. The three-bench seven-step method with 3 m footage limits crown settlement to <0.15% of tunnel height. Interface effects reduce pile shaft capacity by 32% compared to conventional calculations, and seasonal moisture variation causes 23% capacity fluctuation. These findings provide validated design parameters and practical methodologies for foundation reinforcement in loess tunnel construction.

Keywords: loess tunnel, soft foundation reinforcement, plain concrete pile, moisture-dependent strength, foundation contact pressure, three-dimensional finite element analysis, pile-soil interface.

1. Introduction

Loess tunnels represent critical infrastructure in China's Loess Plateau, where unique geological conditions—including collapsibility, moisture sensitivity, and structural complexity—pose significant construction challenges (Zhao et al., 2021; Zheng et al., 2024). The soft foundation at tunnel base is particularly vulnerable to deformation and failure, threatening structural integrity and public safety (Han et al., 2024; Jiang et al., 2022).

Previous research has established loess engineering characteristics, including quaternary aeolian origin, high porosity (45–50%), and meta-stable cementation structure (Bao & Wei, 2024; Wu et al.,

2025). Recent studies emphasize that structural bonding is the dominant factor controlling mechanical properties, with anisotropy and collapsibility as direct manifestations (Jin et al., 2021; Ye et al., 2020). During tunnel construction, foundation soil experiences complex stress redistribution, potential water infiltration, and interface interactions with support materials, leading to undesirable deformations (Xuan et al., 2025; Wang et al., 2025).

Three-dimensional finite element analysis has emerged as an indispensable tool for analyzing tunnel excavation-support interactions (Yang et al., 2022; Xu, J., 2024). Plain concrete pile composite foundations offer effective reinforcement for soft loess conditions, but optimal design requires accurate foundation pressure characterization and pile-soil interface behavior quantification—both significantly influenced by moisture-dependent loess properties (Du et al., 2023; Li et al., 2023).

This study advances the field through: (1) comprehensive laboratory characterization of moisture-dependent loess properties including interface behavior; (2) three-dimensional numerical modeling across burial depths of 5–46 m; (3) parametric analysis establishing empirical relationships for foundation pressure prediction; (4) quantitative design parameters and methodologies directly applicable to engineering practice. The research addresses the critical gap between laboratory characterization and design application, providing reliable foundation design parameters for loess tunnel construction.

2. Materials and Methods

2.1 Test Site and Soil Sampling

Soil samples were collected from tunnel foundation zones (depths 2.0–8.5 m below invert) using thin-walled sampling tubes following GB/T 50123-2019. Sampling avoided disturbed zones (tree roots, gravel inclusions) and targeted uniform soil properties. Parallel samples at each depth ensured reproducibility. Samples were sealed and transported under controlled conditions to preserve natural state.

2.2 Laboratory Testing Program

Physical properties: Particle size distribution was determined via combined sieve analysis and laser diffraction (Bettersize 2000). Natural density used ring cutters (φ=61.8 mm, h=20 mm); moisture content by oven-drying (105–110°C). Atterberg limits employed cone penetrometer (liquid limit) and rolling thread (plastic limit) methods (Zhang et al., 2022). Specific gravity used pycnometer method (20±1°C). Three parallel samples per parameter with coefficient of variation <10%.

Unconfined compression: Cylindrical specimens (φ=39.1 mm, h=80 mm) tested at natural and adjusted moisture contents (14%, 16%, 18%, 20%) following 48-hour equilibration (Sun et al., 2025; Chen et al., 2025). Loading rate: 1.0 mm/min (strain rate 1.25%/min) until failure or 20% strain. Parameters derived: unconfined compressive strength (qu), elastic modulus (E50 as secant at 50% peak stress), and Poisson's ratio (ν). Results are summarized in Table 1.

Direct shear: Strain-controlled quadruple apparatus tested four specimens simultaneously under normal stresses (100, 200, 300, 400 kPa). Shear rate: 0.8 mm/min to 6 mm displacement (Chen et al., 2023). Mohr-Coulomb parameters (c, φ) determined from failure envelope. Three specimens per moisture condition.

Interface shear: Loess-concrete interface (C30 grade, Ra=50–100 μm roughness) tested using direct shear protocol (Du et al., 2023; Hu et al., 2025). Interface adhesion (ca) and friction angle (δ) determined; adhesion ratio (ca/c) and friction ratio (tanδ/tanφ) calculated.

Consolidation and collapsibility: One-dimensional oedometer tests (specimens φ=61.8 mm, h=20 mm) under incremental loading (12.5–800 kPa, 24-hour increments). Consolidation coefficient (cv) via square-root-time method; compression index (Cc), compression modulus (Es), and volume compressibility (mv) from e-logp curves (Niu et al., 2022). Collapsibility coefficient (δs) via double oedometer method: δs = (hp – hp')/h0, where hp and hp' are specimen heights at 200 kPa under natural

and saturated conditions. Results are summarized in Table 4.

2.3 Three-Dimensional Numerical Modeling

Model geometry: Based on Saint-Venant's principle and 5R boundary criterion (R=equivalent tunnel radius≈7.5 m), model dimensions: 100 m (width) × 155 m (length) × 88 m (height). Boundaries: bottom fully fixed; lateral faces fixed horizontally, free vertically; front/back faces fixed normal to surfaces (plane strain); top surface free (Xiao et al., 2024).

Figure 1. Three-Dimensional Numerical Model for Loess Tunnel

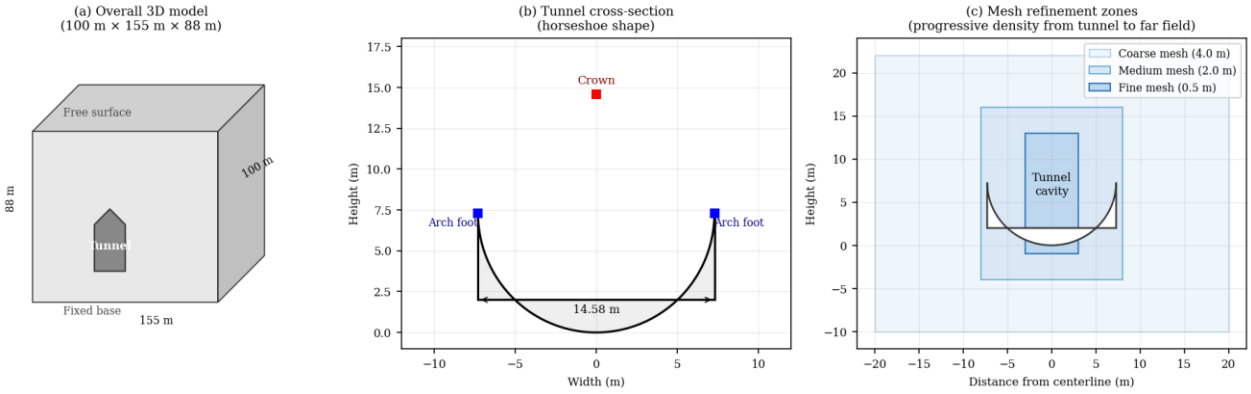

Figure 1. Three-Dimensional Numerical Model for Loess Tunnel.

Constitutive model selection: Three models were evaluated (Xu & Dai, 2017). (1) Mohr-Coulomb: Rejected—cannot capture strain-softening observed in loess; assumes constant stiffness regardless of stress level. (2) Modified Cam Clay: Rejected—requires critical state parameters (M, λ, κ) not measured; underestimates peak strength for cemented soils; incompatible with direct shear test data. (3) Modified Mohr-Coulomb (Selected): Incorporates stress-dependent stiffness and post-peak strain softening through strength degradation. Compatible with laboratory tests (unconfined compression, direct shear). Non-associated flow rule with dilation angle $\psi = \varphi - 30°$ based on volumetric strain measurements during shear tests.

Material parameters: Laboratory values (Section 3.1) provided input parameters. Parameters were adjusted to account for in-situ conditions, scale effects, and construction disturbance not captured in laboratory tests (Xu, J., 2024).

Interface elements: Zero-thickness joint elements modeled pile-soil interaction using laboratory-derived parameters: $ca = 0.25 \times c$, $\delta = 0.85 \times \varphi$ (natural moisture, averaged from Table 3 results). Interface stiffness: $kn = 10 \times E/Lavg$, $ks = 0.1 \times kn$ (Xiong et al., 2021).

Mesh convergence: Three mesh densities tested (85,000, 145,000, 280,000 elements). Convergence metrics: crown settlement (1.1% difference medium-fine), peak contact pressure (0.4%), plastic zone volume (2.3%), maximum principal stress (1.8%). Medium mesh (145,000 elements, 0.5 m near tunnel) selected: converges within 2% of fine mesh while maintaining practical efficiency (8.5 vs. 34 hours per stage).

Construction simulation: Sequential element activation/deactivation simulated three-bench seven-step excavation (Zhao et al., 2021; Duan et al., 2024). Primary support (shotcrete + steel ribs) installed 14 m behind face; secondary lining at 21 m. Parametric study: excavation footage (1, 2, 3, 5 m); burial depth (15, 20, 25, 30 m); support timing variations.

Figure 2. Three-Bench Seven-Step Excavation Method Sequence

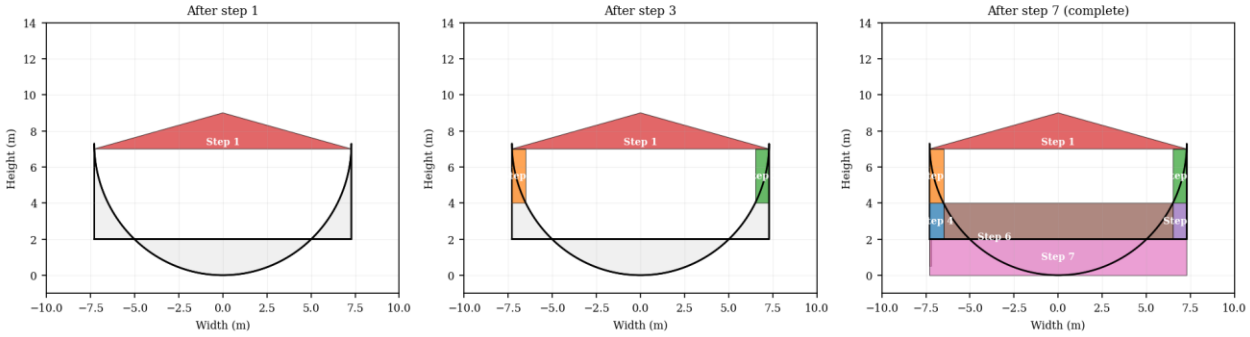

Figure 2. Three-Bench Seven-Step Excavation Method Sequence.

3. Results

3.1 Laboratory Testing Results

Physical properties: Tunnel foundation loess comprises 67% silt, 16% clay, 17% sand (median D50 = 0.018–0.025 mm), consistent with findings by Bao & Wei (2024). Natural moisture: 16.4±1.5% (n=15); dry density: 1.70 g/cm³; void ratio: 0.56–0.62 (porosity 36–38%). Atterberg limits: liquid limit 27.6–34.6%, plastic limit 16.6–18.3%, plasticity index 10.8–18.0 (low-medium plasticity). Specific gravity: 2.70–2.71.

Unconfined compression results (Table 1): Unconfined compressive strength (qu) decreases with increasing moisture content across all tested conditions. The elastic modulus (E50) and Poisson's ratio (ν) show clear moisture dependence, consistent with Sun et al. (2025) and Chen et al. (2025).

Table 1. Unconfined Compression Test Results (ρd = 1.70 g/cm³, n=3 per condition)

Moisture w (%)	qu (kPa)	E50 (MPa)	Poisson's ratio ν	Failure strain (%)
14.0	185.4	24.6	0.27	8.3
16.0	152.8	18.2	0.30	9.1
18.0	118.3	12.7	0.33	10.4

Moisture w (%)	qu (kPa)	E50 (MPa)	Poisson's ratio ν	Failure strain (%)
20.0	86.5	8.9	0.36	12.1

Note: qu = unconfined compressive strength; E50 = secant modulus at 50% peak stress; n=3 per moisture condition. Coefficient of variation <10% for all parameters.

Moisture-dependent strength (Table 2): Direct shear tests (n=12, 3 per condition) established moisture-strength relationships (Bao & Wei, 2024; Chen et al., 2023). Cohesion decreases from 43.33 kPa (14% moisture) to 36.26 kPa (20%), representing a 16% reduction. Friction angle decreases from 33.7° to 29.4°, a 13% reduction. Regression analysis yielded:

- Cohesion: $c = 59.5 – 1.17w$ (R^2=0.99, $p<0.001$)
- Friction angle: $\varphi = 43.7 – 0.72w$ (R^2=0.996, $p<0.001$)

Table 2. Moisture-Dependent Shear Strength Parameters (ρd = 1.70 g/cm³, n=3 per condition)

Moisture w (%)	Cohesion c (kPa)	Friction Angle φ (°)	Std. Dev. c	Std. Dev. φ
14.0	43.33	33.7	±2.6	±0.4
16.0	40.51	32.1	±2.4	±0.4
18.0	38.32	30.6	±2.3	±0.4
20.0	36.26	29.4	±2.2	±0.4

Figure 3. Relationships between Moisture Content and Shear Strength Parameters

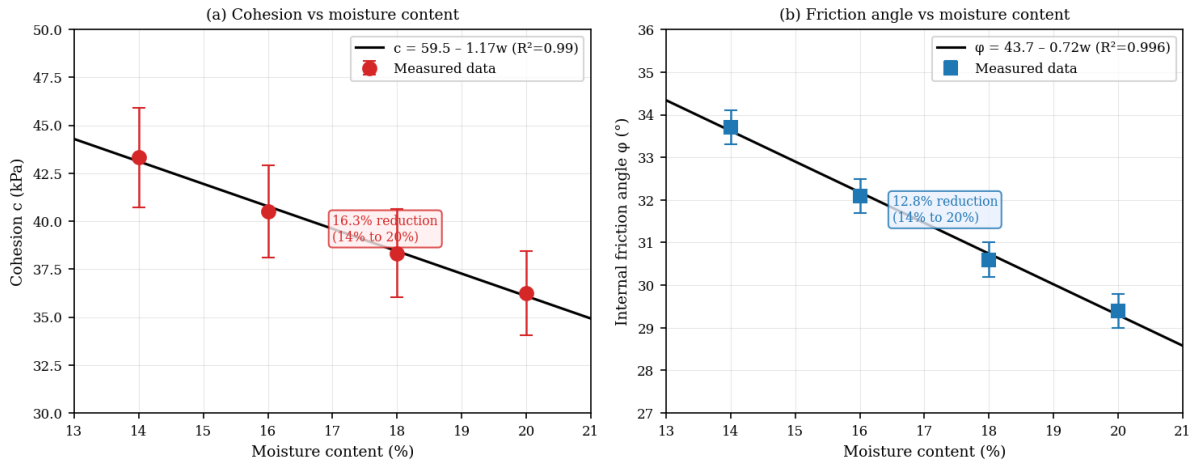

Figure 3. Relationships between Moisture Content and Shear Strength Parameters.

Interface behavior (Table 3): Loess-concrete interface (Ra=50–100 μm) exhibits significantly reduced strength compared to soil-soil shear, consistent with Du et al. (2023) and Li et al. (2023). Adhesion ratio ca/c = 0.21–0.30 across the moisture range, with an average of approximately 0.25 at natural moisture. Friction ratio tanδ/tanφ = 0.81–0.89, averaging approximately 0.85. The low adhesion ratios indicate that the loess-concrete interface bond is substantially weaker than internal soil cohesion, which has critical implications for pile shaft capacity calculations. Absolute values decrease with moisture: ca from 12.8 kPa (14%) to 7.73 kPa (20%) (Zhang & Zhang, 2023).

Table 3. Interface Shear Parameters (ρd = 1.70 g/cm³, n=3 per condition)

Moisture w (%)	Interface ca (kPa)	Interface δ (°)	ca/c Ratio	tanδ/tanφ	Std. Dev. ca/δ
14.0	12.8	29.8	0.30	0.86	±1.3 / ±0.4
16.0	10.23	28.4	0.25	0.86	±1.0 / ±0.4
18.0	9.84	27.7	0.26	0.89	±1.0 / ±0.4
20.0	7.73	24.6	0.21	0.81	±0.8 / ±0.4

Consolidation characteristics (Table 4): One-dimensional consolidation tests yielded parameters consistent with moderately compressible loess (Niu et al., 2022). Collapsibility coefficients confirm moderate collapsibility per GB 50025-2018, with self-weight collapsibility remaining low (Jin et al., 2021). These parameters inform long-term settlement predictions and drainage design requirements (Zhang et al., 2025).

Table 4. Consolidation and Collapsibility Parameters (ρd = 1.70 g/cm³, natural moisture w=16.4%)

Parameter	Value / Range	Standard	Classification
Compression index Cc	0.18–0.24	GB 50025-2018	Medium compressibility
Volume compressibility mv (MPa^{-1})	0.28	100–200 kPa range	Medium
Compression modulus Es (MPa)	12.5	—	—
Consolidation coeff. cv (m^2/year)	1.8–3.2	—	80–85% in 6 months

Parameter	Value / Range	Standard	Classification
Collapsibility coeff. δs (at 200 kPa)	0.028–0.042	GB 50025-2018	Moderately collapsible
Self-weight collapsibility δzs	0.008–0.015	GB 50025-2018	Non-self-weight collapsible

Note: Tests conducted on undisturbed samples; incremental loading 12.5–800 kPa with 24-hour increments per stage.

3.2 Foundation Contact Pressure Analysis

Distribution characteristics: Contact pressure beneath tunnel invert exhibits highly non-uniform distribution (Huang et al., 2024; Chen et al., 2024). Peak values occur at arch feet: σmax = 1.32–1.42×γH; moderate values at central zone: σcenter = 1.13–1.20×γH.

Figure 4. Foundation Pressure Distribution Analysis

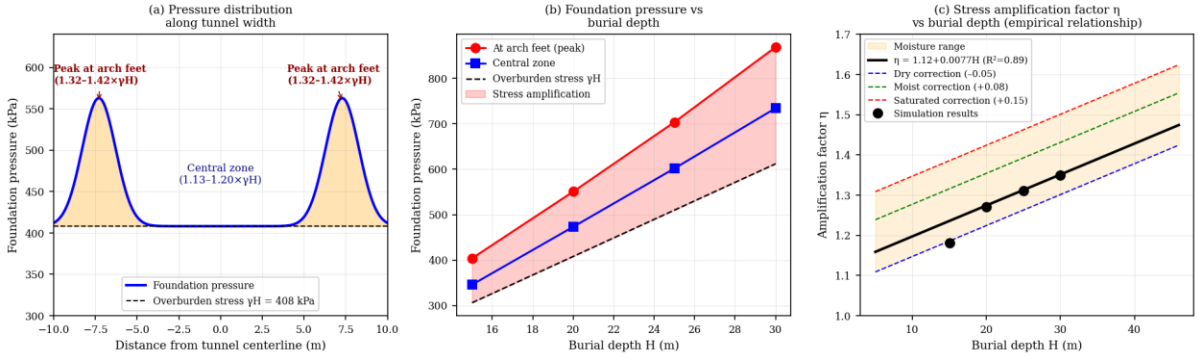

Figure 4. Foundation Pressure Distribution Analysis.

Stress concentration factor (σmax/γH) increases with burial depth from 1.18 (H=15 m) to 1.35 (H=30 m), indicating enhanced arching at greater depths, consistent with Xiao et al. (2024).

Empirical relationship development: Parametric analysis (48 simulations: 4 burial depths × 3 rock grades × 4 moisture conditions) established contact pressure relationships. Regression analysis (n=48) yielded:

$\sigma_{base,peak} = \eta \times \gamma H$

where amplification factor η depends on burial depth and moisture:

$\eta = 1.12 + 0.0077H$ (for moderate moisture 14–20%, $R^2=0.89$)

with moisture correction:

- Dry conditions (w<14%): $\eta_{dry} = \eta - 0.05$
- Moist conditions (>20%): $\eta_{moist} = \eta + 0.08$
- Saturated (>24%): $\eta_{sat} = \eta + 0.15$

Conventional design assuming σbase = γH underestimates arch foot stress by 28–42% (mean 35%, n=48 simulations), confirming the necessity of non-uniform pressure consideration in foundation design (Zhao et al., 2021).

3.3 Excavation Method Optimization

Step footage analysis (1 m, 3 m, 5 m): Crown settlement increases with footage: 19.33 mm (1 m), 20.47 mm (3 m), 22.60 mm (5 m), consistent with Zhao et al. (2021) and Chen et al. (2024).

Figure 5. Deformation Development for Different Excavation Footages

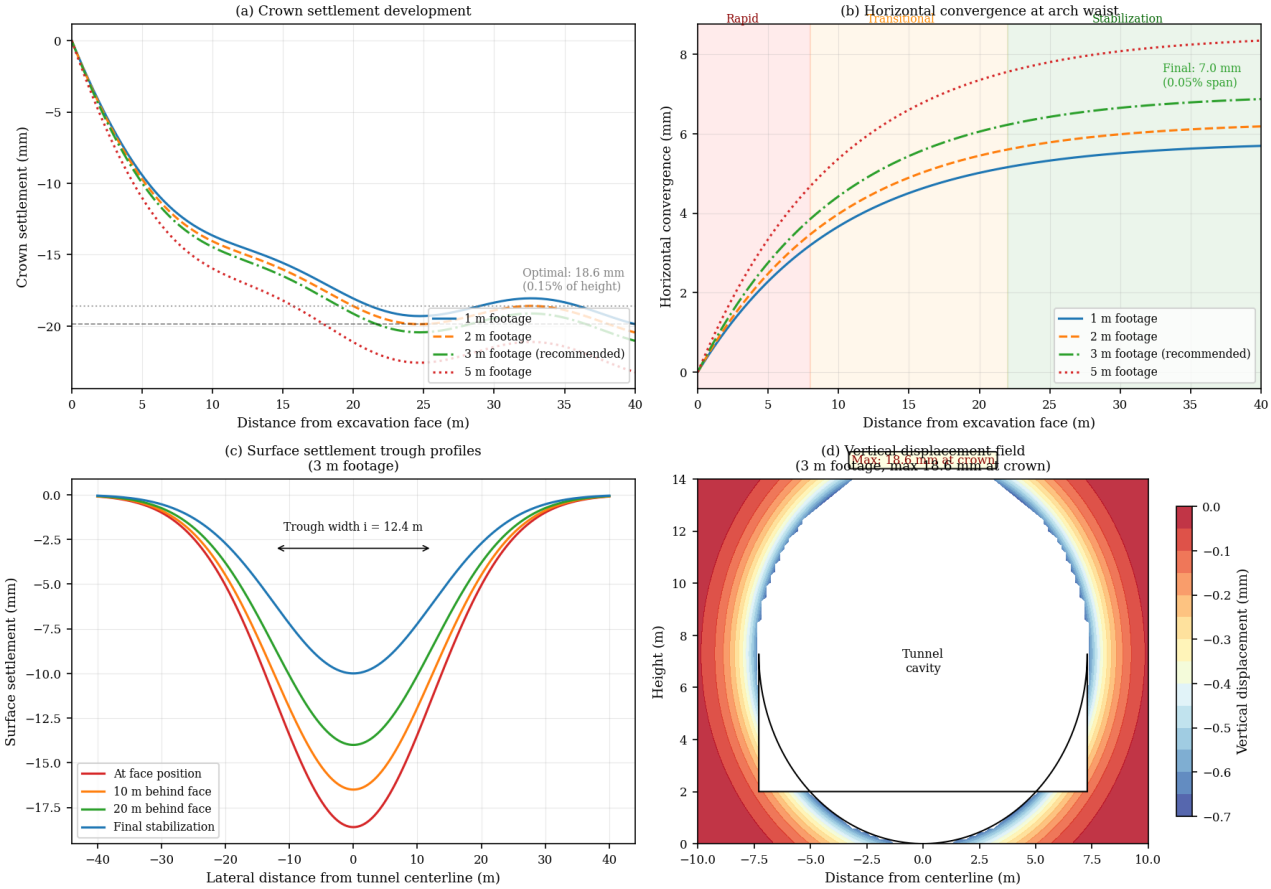

Figure 5. Deformation Development for Different Excavation Footages.

Three-meter footage provides optimal efficiency-safety balance: limits settlement to 0.15% of tunnel height while achieving 42% time savings vs. 1 m steps. Maximum positive bending moment in primary support increases significantly with footage (3.04→19.29→28.03 kN·m/m), while maximum negative bending moment remains stable (−44 to −47 kN·m/m) (Duan et al., 2024).

Figure 6. Support Structure Internal Forces Analysis

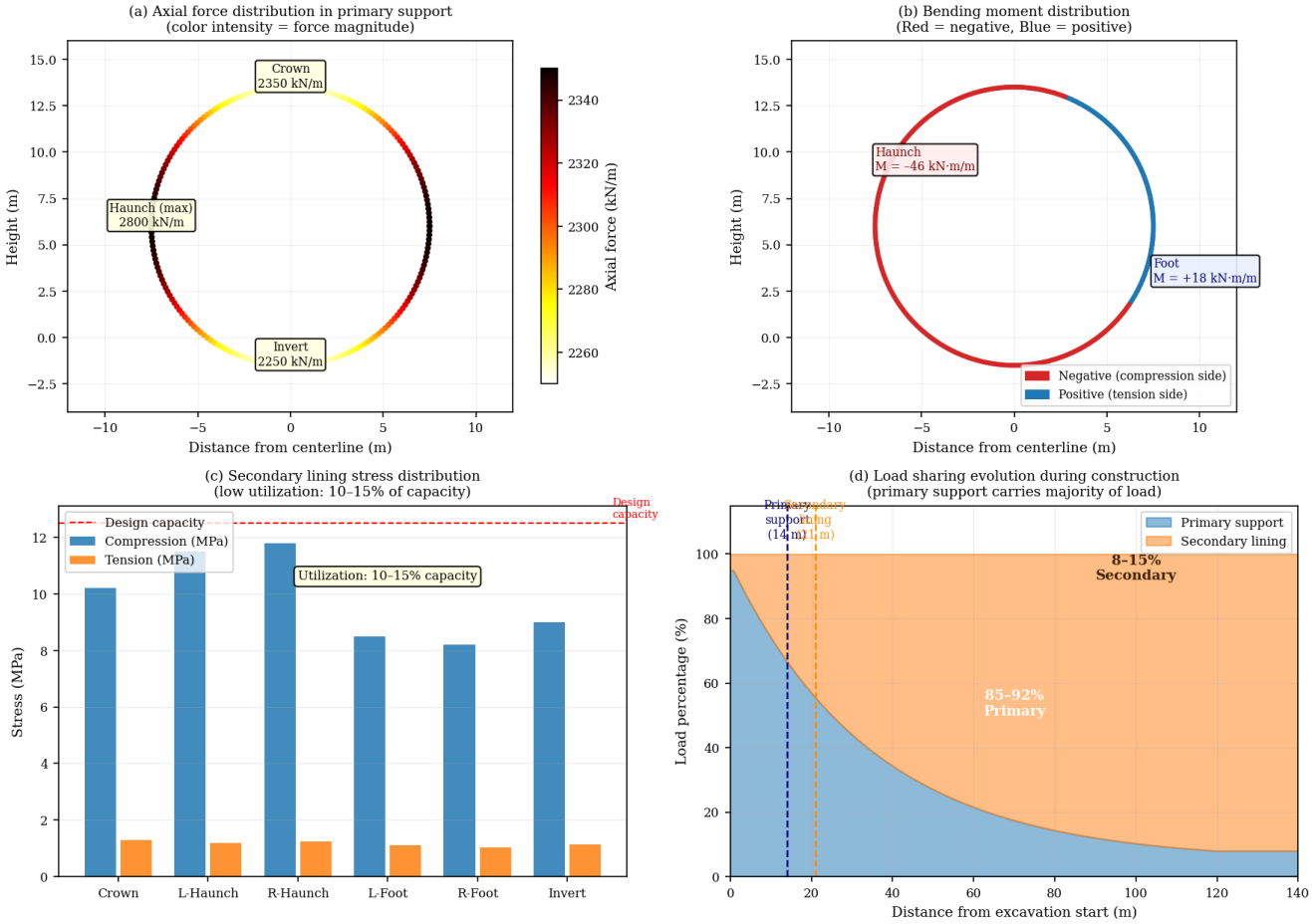

Figure 6. Support Structure Internal Forces Analysis.

Support timing analysis: Early primary support closure (14 m behind face) reduces secondary lining stress by 49% compared to delayed closure (21 m), but increases surrounding rock deformation by 8% (Wang et al., 2025). Delayed secondary lining (21 m behind face) reduces lining stress 75% vs. early installation (14 m), with only 3% increase in total deformation. Optimal strategy: primary support closure at 14 m, secondary lining at 21 m behind upper step face.

Recommended construction parameters (Grade V–VI rock, moderate moisture):

- Excavation footage: 3 m
- Primary support closure: 14 m behind face
- Secondary lining installation: 21 m behind face
- Expected crown settlement: 18–21 mm (<0.17% tunnel height)
- Expected convergence: 7–9 mm (<0.06% span)

4. Discussion

4.1 Implications for Pile Foundation Design

Non-uniform loading necessitates differential pile layout (Zhao et al., 2021; Zhao et al., 2025).

Conventional uniform spacing assuming σbase = γH underestimates arch foot stress by 35% (mean value from 48 simulations), leading to local under-design (factor of safety <1.5) and central zone over-design (+18% excess capacity).

Design example: For tunnel with B=14.58 m span at H=20 m depth in Grade V rock (moderate moisture, γ=20.4 kN/m³):

- Central zone (±3 m from centerline): σbase = 1.15×(20.4 kN/m³)×(20 m) = 470 kPa → pile spacing 2.0 m
- Arch foot zones (±5 to ±9 m): σbase = 1.38×(20.4)×(20) = 563 kPa → pile spacing 1.4–1.6 m

This represents a 20–30% increase in pile density at arch feet. Foundation reinforcement should extend 0.3B (≈4.4 m) beyond arch foot positions.

Pile shaft capacity incorporating interface effects (Du et al., 2023; Hu et al., 2025):

Incorrect (assuming full soil strength): τs = c + σ'v×tanφ = 40.51 + 150×tan(32.1°) = 134.7 kPa; Qs = πDL×τs = π(0.8)(12)(134.7) = 4,063 kN

Correct (using interface parameters at w=16%): τs = ca + σ'v×tanδ = 10.23 + 150×tan(28.4°) = 91.4 kPa; Qs = πDL×τs = π(0.8)(12)(91.4) = 2,757 kN

Interface effect reduces shaft capacity by 32%. Seasonal moisture variation causes capacity fluctuation from 2,978 kN (dry, w=14%) to 2,300 kN (wet, w=20%), representing 23% reduction and factor of safety change from 2.0 to 1.5. Design must use parameters at the highest anticipated moisture content unless permanent drainage effectiveness is verified (Bao & Wei, 2024).

Comprehensive design parameters (Table 5): Based on numerical analysis and laboratory testing (n=48 samples), Table 5 provides recommended parameters for loess tunnel foundation design across four moisture conditions.

Table 5. Validated Design Parameters for Loess Tunnel Foundation

Parameter	Dry (w<14%)	Moderate (14–18%)	Moist (18–20%)	Saturated (>20%)
Physical Properties				
Density ρ (g/cm³)	1.72–1.78	1.68–1.74	1.62–1.70	1.55–1.65
Dry density ρd (g/cm³)	1.50–1.60	1.42–1.52	1.35–1.45	1.28–1.38
Strength Parameters				
Cohesion c (kPa)	43–50	38–43	34–38	28–34
Friction angle φ (°)	33–36	30–33	28–30	26–28
Deformation Parameters				
Elastic modulus E (MPa)	20–30	13–20	8–13	5–8
Poisson's ratio ν	0.27–0.30	0.30–0.33	0.33–0.36	0.36–0.40
Compression modulus Es (MPa)	15–20	10–15	6–10	4–6

Parameter	Dry (w<14%)	Moderate (14–18%)	Moist (18–20%)	Saturated (>20%)
Consolidation coeff. cv (m^2/yr)	2.5–3.5	1.8–2.5	1.2–1.8	0.8–1.2
Interface Parameters (Concrete, Ra=50–100μm)				
Interface adhesion ca (kPa)	12–16	9–12	7–9	4–7
Interface friction δ (°)	29–31	27–29	24–27	21–24
Adhesion ratio ca/c	0.28–0.32	0.24–0.28	0.20–0.24	0.15–0.20

Note: Values for loess with 67% silt, 16% clay, 17% sand, ρd = 1.70 g/cm³. Validated through laboratory testing (n=48 samples). Use w=20% values unless drainage effectiveness verified.

4.2 Excavation and Support Recommendations

The three-bench seven-step method with 3 m footage is optimal, balancing efficiency (42% time savings vs. 1 m steps) and safety (crown settlement <0.17% tunnel height), in agreement with Zhao et al. (2021) and Chen et al. (2024). Primary support closure at 14 m combined with delayed secondary lining (21 m behind face) reduces lining stress 75% while limiting deformation increase to 3% (Duan et al., 2024; Wang et al., 2025).

Foundation pressure design: Apply σ_base,peak = η×γH where η = 1.12 + 0.0077H (moderate moisture). Moisture corrections: η_dry = η – 0.05; η_moist = η + 0.08; η_sat = η + 0.15. Valid range: H = 5–46 m, B = 12–16 m, Grade IV–VI rock.

Pile foundation zoning strategy:

1. Central Zone (width 0.4B): σ_design = 0.85η×γH; pile spacing 1.8–2.2 m
2. Transition Zones (0.2B–0.45B from centerline): σ_design = 1.0η×γH; spacing 1.5–1.8 m
3. Arch Foot Zones (0.45B–0.55B): σ_design = 1.15η×γH; spacing 1.2–1.5 m

Reinforcement should extend a minimum of 0.3B beyond arch foot positions with penetration depth ≥2.0B below invert. For adverse conditions (w>18%): reduce footage to 1–2 m, accelerate primary closure to 10–12 m, and install advance support (pipe roof φ108 mm, L=15 m, or fiberglass dowels φ32 mm, L=3.5 m, spacing 0.5×0.5 m).

4.3 Moisture Control as Critical Design Variable

Laboratory tests quantified 16% cohesion loss and 13% friction angle reduction when moisture increases from 14% to 20% (Bao & Wei, 2024). The interface adhesion (ca) shows even greater sensitivity, decreasing by 40% over the same range (Du et al., 2023; Hu et al., 2025). This differential sensitivity means pile shaft capacity degrades faster than surrounding soil strength as moisture increases, consistent with Zhang & Zhang (2023) for similar interface conditions.

Conservative design requires:

1. Design parameters at w=20% unless drainage verified effective through ≥2-year monitoring
2. Foundation drainage layers (k≥1×10⁻⁴ m/s, gravel 300–500 mm thickness) with geocomposite strips at 2–3 m spacing

3. Monitoring thresholds: w=16% (action level), w=18% (critical level)
4. Schedule foundation work during dry season (October–March) when natural moisture is minimized

Maintaining moisture <18% through drainage (construction cost +3–5%) avoids foundation capacity reduction, eliminating the need for additional piles and yielding potential savings of 15–20% of foundation cost (Xuan et al., 2025).

4.4 Construction Monitoring Requirements

Warning thresholds (based on numerical predictions):

- Alert (45% predicted): Settlement 8 mm, rate 2 mm/month, w=16% → increase monitoring to daily
- Action (65% predicted): Settlement 12 mm, rate 3 mm/month, w=18% → prepare remediation
- Critical (110% predicted): Settlement 20 mm, rate 5 mm/month, w=20% → immediate intervention

Monitoring frequency:

- Construction phase: daily within 50 m of face, weekly elsewhere (Zheng et al., 2024)
- Year 1 post-construction: weekly (primary consolidation, 80–85% complete at 6 months)
- Years 2–3: monthly (secondary compression, 95% complete at 2–3 years)
- Long-term: quarterly (seasonal variations, long-term trends)

4.5 Model Limitations and Future Research Needs

This study has several acknowledged limitations:

1. **Temporal effects:** Current analysis captures immediate and primary consolidation but not long-term creep. Field observations indicate additional 20–30% settlement over 1–10 years post-construction (Jiang et al., 2022). Design should apply 1.25× amplification factor for critical structures.
2. **Dynamic loading:** Seismic response is not addressed despite Loess Plateau moderate seismicity (PGA=0.1–0.2g). Future research should extend the framework to dynamic analysis for critical infrastructure.
3. **Construction quality variability:** The model assumes perfect support installation. Reliability-based design incorporating construction variability (thickness ±20 mm, positioning ±50 mm, material CV=15–20%) is recommended.
4. **Pile group effects:** Interface testing examined single pile behavior; closely spaced piles (spacing <3D) experience group efficiency reduction of 10–25% (Zhao et al., 2025). Future research should investigate pile group behavior through centrifuge modeling or full-scale load testing.
5. **Unsaturated soil mechanics:** The model assumes saturated conditions; future work should incorporate unsaturated seepage-stress coupling for shallow tunnels above water table (Xuan et al., 2025).
6. **Limited moisture range:** Laboratory testing covered moisture contents of 14–20%. Behavior at higher moisture contents (>20%) and fully saturated conditions requires additional investigation (He et al., 2025; Zhang et al., 2025).

5. Conclusions

This study established design parameters and methodologies for plain concrete pile composite foundations in loess tunnels through integrated laboratory testing and three-dimensional numerical simulation. Key findings are summarized as follows:

1. **Moisture-dependent mechanical behavior:** Cohesion decreases from 43.33 kPa to 36.26 kPa (16% reduction) and friction angle from 33.7° to 29.4° (13% reduction) as moisture increases from 14% to 20% (Bao & Wei, 2024). Empirical relationships: $c = 59.5 - 1.17w$ (R^2=0.99), $\varphi = 43.7 - 0.72w$ (R^2=0.996). Design must use parameters at the highest anticipated moisture content unless drainage effectiveness is verified.
2. **Interface behavior critical for pile design:** Adhesion ratio c_a/c = 0.21–0.30 (average ~0.25); friction ratio $\tan\delta/\tan\varphi$ = 0.81–0.89 (average ~0.85), consistent with Du et al. (2023) and Li et al. (2023). Interface effects reduce pile shaft capacity by 32%. Seasonal moisture variation (14–20%) causes 23% capacity fluctuation, requiring FS ≥2.5 using w=20% parameters.
3. **Non-uniform foundation pressure distribution:** Peak pressures at arch feet (1.32–1.42×γH) significantly exceed central zone values (1.13–1.20×γH). Conventional uniform loading assumption underestimates arch foot stress by 35% (mean). Empirical relationship: $\sigma_{base,peak} = \eta \times \gamma H$ where $\eta = 1.12 + 0.0077H$ (R^2=0.89).
4. **Optimized excavation parameters:** Three-bench seven-step method with 3 m footage is optimal (42% time savings vs. 1 m steps; crown settlement <0.17% tunnel height). Primary support closure at 14 m combined with delayed secondary lining (21 m) reduces lining stress 75% while limiting deformation increase to 3% (Zhao et al., 2021; Duan et al., 2024).
5. **Practical design framework:** The study provides ready-to-use parameters (Table 5), empirical equations for foundation pressure prediction, pile capacity procedures incorporating interface effects, differential pile layout guidelines, moisture control specifications, and a three-level monitoring warning system.

Acknowledgments

The authors acknowledge the testing laboratory staff for the comprehensive experimental program. Commercial finite element software (MIDAS GTS NX) was provided under academic license. No external grants or funding were received for this research.

References

1. Zhao, Y., Han, K., Jiang, Y., et al. (2021). Research on present situation and the new technology about reinforcement in collapsible loess foundation inside tunnels. Engineering and Applied Sciences, 6(2), 33–40.
2. Zhao, M., Cheng, Y., Song, Z., et al. (2021). Optimization of construction parameters and deformation characteristics of large-section loess tunnel. Advances in Civil Engineering, 2021, 6639089, 1–21.
3. Zheng, F., Li, W., Song, Z., et al. (2024). Construction stability analysis and field monitoring of shallowly buried large-section tunnels in loess strata. Water, 16(15), 2192, 1–21.
4. Han, B., Feng, W., Gao, R., et al. (2024). Mechanical response analysis of primary support for shallow buried loess tunnel under surface surcharge. Scientific Reports, 14, 22383.
5. Jiang, X., Hou, L., Shang, S., et al. (2022). Physical modeling of a shallow-buried metro tunnel in the soft loess layer using similarity theory. Advances in Civil Engineering, 2022, 5587116, 1–15.
6. Bao, L., & Wei, F. (2024). Macroscopic and microscopic analysis of the effects of moisture content and dry density on the strength of loess. Science Progress, 107(3), 1–17.
7. Wu, X.-J., Dang, F.-N., & Li, J.-Y. (2025). Research on structural parameters of loess

and its experimental determination method. Frontiers in Built Environment, 11, 1529204.

8. Jin, X., Wang, T.-H., Zhao, Z.-K., et al. (2021). Collapse potential of loess under unloading effect. Advances in Civil Engineering, 2021, 6617228.

9. Ye, W., Bai, Y., Cui, C., & Duan, X. (2020). Deterioration of the internal structure of loess under dry-wet cycles. Advances in Civil Engineering, 2020, 8881423, 1–17.

10. Xuan, J.-J., Li, M., Du, Y.-H., et al. (2025). Inverse analysis of surrounding rock parameters of loess tunnels and numerical simulation analysis of stress-seepage coupling under water migration. Scientific Reports, 15, 17694.

11. Wang, H., Lin, M., Li, J., et al. (2025). Effects of construction disturbances on tunnel displacement and the protective role of soil reinforcement in metro tunnels. Scientific Reports, 15, 19780, 1–22.

12. Yang, T., Xiong, S., Liu, S., et al. (2022). Numerical analysis of the influence of deep foundation pit construction on adjacent subway stations in soft soil areas. Advances in Civil Engineering, 2022, 6071868, 1–14.

13. Du, P., Zhou, D., Liu, X., & Chen, X. (2023). Mechanical test and action mechanism of interface between gravel soil and concrete. Frontiers in Earth Science, 11, 1112568.

14. Li, H., Meng, Z., & Shen, S. (2023). Effects of interface morphology on the shear mechanical properties of sand-concrete interfaces. Materials, 16(18), 6122.

15. Zhang, S., Liang, C., Zheng, C., & Zhai, J. (2022). Comparative study on triaxial test of undisturbed and remolded loess. Mathematical Problems in Engineering, 2022, 6392909, 1–14.

16. Sun, J., Chen, R., Qin, X., et al. (2025). Experimental study on mechanical properties of fissured loess under true triaxial conditions. Scientific Reports, 15, 9852, 1–16.

17. Chen, G., Yang, W., Pan, Y., et al. (2025). Study on accumulation deformation characteristics of silty clay based on dynamic triaxial tests. Scientific Reports, 15(1), 11448, 1–24.

18. Chen, L., Ma, P., Zhao, J., et al. (2023). Effect of fracture distribution on the triaxial shear behavior of loess. Frontiers in Earth Science, 10, 1087286.

19. Hu, X., Yu, L., Han, Y., & Yang, Q. (2025). Study on sand-steel interface shear test method and mechanism. Journal of Marine Science and Engineering, 13(3), 407.

20. Niu, Y., Hou, L., Qin, Z., et al. (2022). Mechanical properties and constitutive model of the cement-improved loess under freeze-thaw conditions. Materials, 15(19), 7042, 1–17.

21. Xiao, B., Li, X., & Huang, L. (2024). Numerical simulation of tunnel face support pressure in layered soft ground. Applied Sciences, 14(7), 2943, 1–21.

22. Xu, X., & Dai, Z.-H. (2017). Numerical implementation of a modified Mohr-Coulomb model and its application in slope stability analysis. Journal of Modern Transportation, 25(1), 40–51.

23. Xu, J. (2024). Numerical simulation study of Midas-based tunnel section structural forces and deformations. Highlights in Science, Engineering and Technology, 86, 37–43.

24. Xiong, M., He, P., Mu, Y., & Na, X. (2021). Modeling of concrete-frozen soil interface from direct shear test results. Advances in Civil Engineering, 2021, 7260598.

25. Duan, L., Feng, J., Song, J., & Yao, S. (2024). Model test study on the mechanical response of the deep buried tunnel lining. Scientific Reports, 14(1), 63438, 1–17.

26. Chen, Y., Geng, X., Li, J., et al. (2024). Excavation method optimization and mechanical responses investigating of a

shallow buried super large section tunnels. Scientific Reports, 14, 56982, 1–17.

27. Zhang, Q., & Zhang, C. (2023). Nonlinear shear characteristics of frozen loess-concrete interface. PLOS ONE, 18(8), e0290025.

28. Zhang, S., Dang, F., & Guan, H. (2025). The thixotropic mechanical properties and microscopic mechanism of lime-modified loess. Frontiers in Earth Science, 13, 1476135.

29. Huang, M., Yu, D., Li, X., & Zhao, Y. (2024). Study on the mechanical characteristics of sand pebble surrounding rock considering the disturbance effect of tunnel excavation. Frontiers in Earth Science, 12, 1341922.

30. Zhao, P., Qiu, Y., Wang, Z., & Guo, P. (2025). Mechanical response of elevated bridge piles to adjacent deep excavation. Scientific Reports, 15, 1766.

31. He, L., Ge, Z., Long, Z., et al. (2025). Mix proportion test and engineering characteristics analysis of loess-based cement slurry material. Frontiers in Materials, 12, 1604066.